RevMexAA (Serie de Conferencias), **7**, 137–142 (1998)

HST/FOS SPECTROSCOPY OF HH47A: SHOCK VELOCITY, MAGNETIC FIELDS, AND SECONDARY SHOCK STRUCTURE

Jason Tumlinson[1,2] and Patrick Hartigan[1]

Jon A. Morse[2]

and

John C. Raymond[3]

RESUMEN

Presentamos nuevas observaciones del *Telescopio Espacial Hubble* con el espectrógrafo de objetos débiles del choque de proa y del disco de Mach de la superficie de trabajo del objeto HH 47A. Un modelo de choque de una sola velocidad paralela al plano, reproduce satisfactoriamente los cocientes observados en las líneas de diagnóstico pero subestima los flujos en las líneas prohibidas. Estos flujos son modelados con mayor precisión al incluir un choque más lento y más pequeño dentro de la proa principal, con emisión superpuesta a la emisión de proa. Este segundo modelo de choque secundario predice con exactitud los cocientes de diagnóstico y flujos de las líneas prohibidas observadas. Confirmamos la naturaleza de la emisión de dos fotones en el continuo azul para el disco de Mach, pero no en el choque de proa, debido a una posible contaminación de luz dispersada.

ABSTRACT

We present new *HST*/Faint Object Spectrograph observations of the bow shock and Mach disk of the HH 47A working surface. A single-velocity, plane-parallel shock model successfully reproduces the observed diagnostic line ratios but underestimates the forbidden line fluxes. These fluxes are most accurately modeled by the addition of a slower, smaller shock inside the main bow, with its emission superimposed on the bow emission. This secondary shock model accurately predicts the diagnostic line ratios and the observed forbidden line fluxes. We confirm the two-photon nature of the blue continuum for the Mach disk but not in the bow shock due to possible scattered light contamination.

Key words: **ISM: JETS AND OUTFLOWS — STARS: FORMATION — STARS: MASS LOSS**

1. OBSERVATIONS AND DATA REDUCTION

We observed the bow shock and Mach disk of the HH 47A working surface to study the physical conditions in these shocks and refine current models of this object. These observations were taken by the Faint Object Spectrograph aboard the *Hubble Space Telescope* in March 1996. The two spectra displayed in Figure 1 are co-added individual spectra taken with the $0.21'' \times 1.71''$ aperture, the `G270H`(UV), `G400H`(optical), `G570H`(red) gratings, and the red side detector. Flux calibration was done by the STScI pipeline. Wavelength calibration of the spectra with standard lamp spectra taken at the time of the science observations improved the pipeline calibration error from 0.2 to 0.08 Å. Lines are not resolved by the $250\,\mathrm{km\,s^{-1}}$ resolution of the instrument. The observed spectral lines were identified and spurious lines were removed by viewing the `MULTIGROUP` data in time sequence. Lines fluxes were calculated using the IRAF routine **splot**. The line fluxes were dereddened with an $E_{(B-V)} = 0.18$, determined from ground based spectra of the nearby Gum Nebula (Morse et al. 1994).

The continuum was sampled with 50 Å bins centered at approximately 50 points in each of the bow shock and Mach disk spectra and chosen to avoid all emission lines. The flux in each bin was dereddened and then

[1]Department of Space Physics & Astronomy, MS 106, Rice University, Houston, TX 77005, USA; jason@rice.edu, hartigan@sparky.rice.edu.

[2]Department of Astrophysical and Planetary Sciences, University of Colorado, Boulder, CO 80309, USA; morsey@casa.colorado.edu.

[3]Harvard-Smithsonian Center for Astrophysics, 60 Garden Street, Cambridge, MA, 02138, USA; jraymond@cfa.harvard.edu.

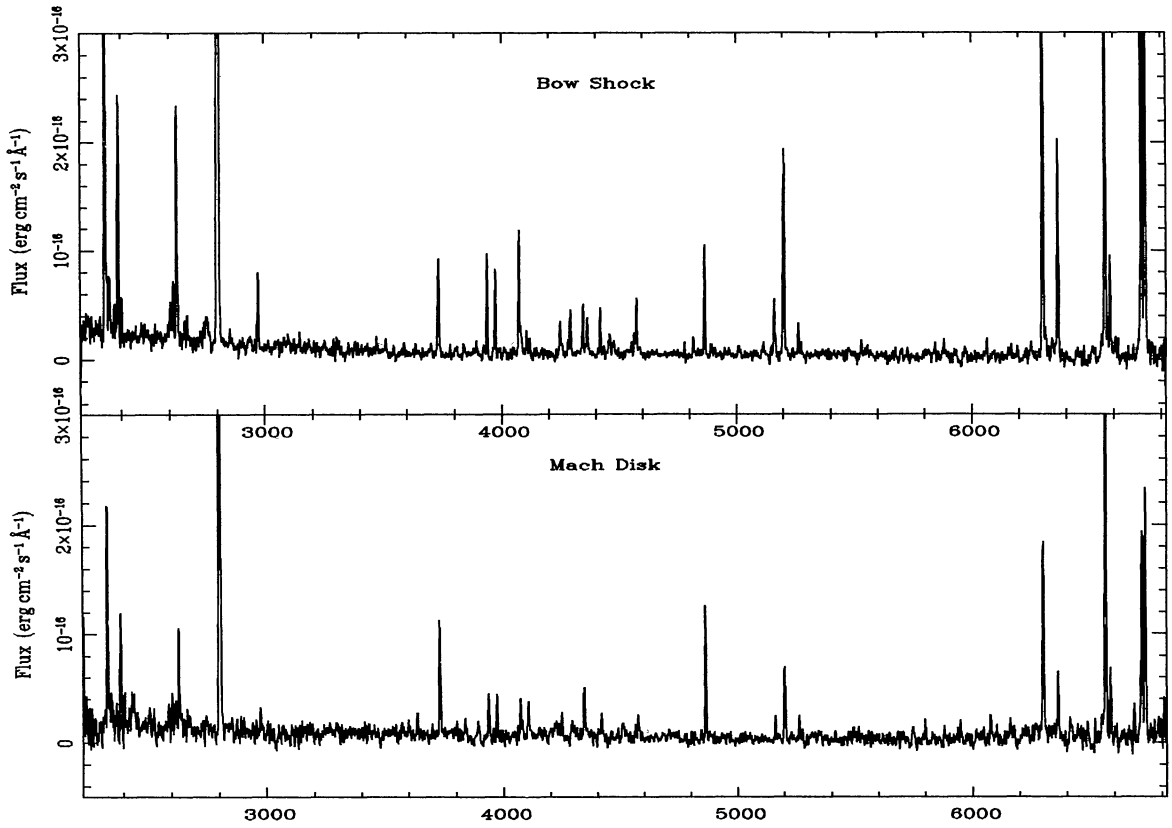

Fig. 1. Spectra of the bow shock and Mach disk of HH 47A, smoothed over 17 Å.

averaged over the 50 Å width of the bins. Plots of these measurements appear in Figure 2. The reduced HH 47 bow shock and Mach disk spectra appear in Figure 1. These spectra have been smoothed by a 17 Å running median filter. Dereddened line fluxes appear in Table 1 with their measurement errors.

2. SHOCK VELOCITY, PRESHOCK DENSITY, AND THE MAGNETIC FIELD

We model these spectra with a plane-parallel shock code that has proven successful at modeling Herbig-Haro objects in the past (Raymond 1979; Hartigan, Morse, & Raymond 1994). This code can be adapted to model bow shocks if the planar models are carefully added together in the correct bow geometry, but even this more sophisticated model cannot take into account the size and shape of the FOS slit. However, the plane-parallel approximation holds reasonable well for this bow shock because the slit was placed near the tip of the bow where the shock velocity (V_s) is at its maximum and does not vary rapidly. We make no attempt to model the Mach disk spectrum since there is an unknown amount of emission from the bow in the beam.

The absence of [O III] 5007 Å emission in the spectrum constrains the shock velocity to less than $100\,\mathrm{km\,s^{-1}}$, where this line becomes bright. The [N I] 6584 Å/Hα line ratio sets the shock velocity to $80\,\mathrm{km\,s^{-1}} \pm 5\,\mathrm{km\,s^{-1}}$, where the error is determined from a 10% variation in the line ratio with changing shock velocity. This V_s is slightly larger than the value of $50-60\,\mathrm{km\,s^{-1}}$ obtained by Morse et al. (1994), who derived their value from spectra that contained more of the bow at lower shock velocities.

The extinction-corrected Hα flux of $4.86 \times 10^{-15}\,\mathrm{erg\,cm^{-2}s^{-1}}$ sets the preshock density for the $80\,\mathrm{km\,s^{-1}}$ model to $\log n_0 = 2.72 \pm 0.35\,\mathrm{cm^{-2}}$. This density is consistent with the $\log n_0 = 3.01 \pm 0.15\,\mathrm{cm^{-2}}$ value determined by Morse et al. (1994). The angle of inclination from the line-of-sight to the shock front, which affects the predicted flux.

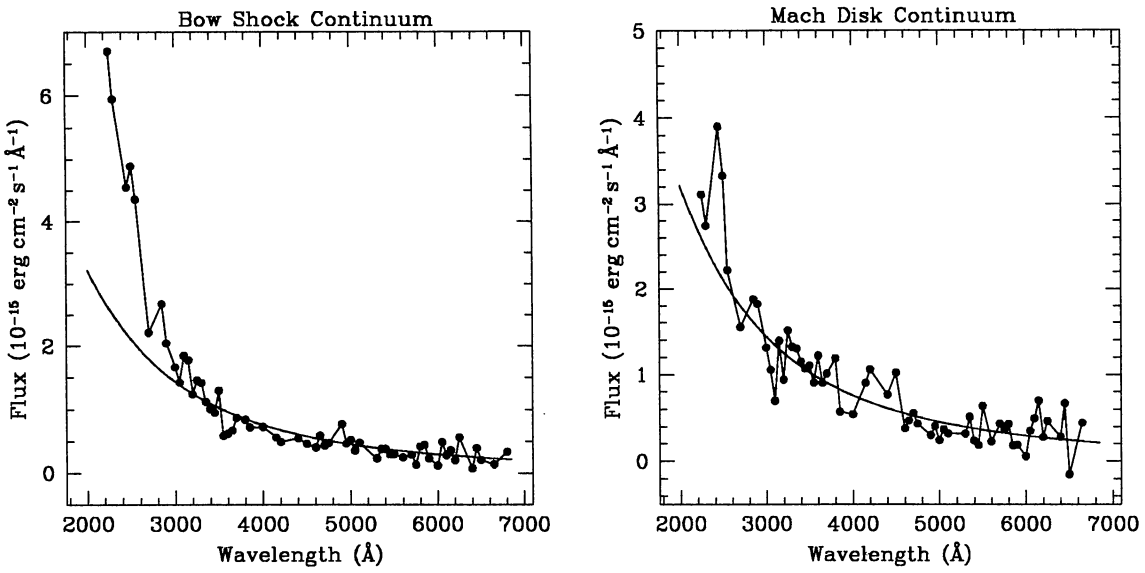

Fig. 2. Averaged and dereddened continua of the bow shock and Mach disk.

With the shock velocity and density fixed at the above values a plane-parallel shock model accurately predicts the [S II]λ6716 Å/[S II]λ6731 Å ratio for a preshock magnetic field of $B_0 = 165\,\mu$G.

3. EVIDENCE FOR SECONDARY SHOCK STRUCTURE

The self-consistent shock parameters $V_s = 80\,\mathrm{km\,s^{-1}} \pm 5\,\mathrm{km\,s^{-1}}$, $\log n_0 = 2.72 \pm 0.35\,\mathrm{cm^{-2}}$, and $B_0 = 165\,\mu$G are taken as the baseline values for further other analysis of this data. Unfortunately, this baseline model predicts mush lower fluxes for low-excitation forbidden lines like [S II] λλ 4070 Å and [N II] λλ 5200 Å than are actually observed. Table 2 shows the forbidden line fluxes and ratios predicted by the baseline model.

HH 47A is a low-excitation shock, with only neutral and singly ionized species in the cooling zone. The low-ionization diagnostics brighten with decreasing shock velocity as the ionization fraction of the shock decreases. This fact and the observed forbidden line ratios strongly suggest that there is a lower velocity shock in the slit along with the main bow. To test this hypothesis we superimposed a lower velocity shock scaled by a small factor (a ∼ 40%) on the baseline model. This model assumes that there is a slower shock inside the main bow that fills a small portion of the aperture beam. The preshock conditions for the secondary shock are taken to be the *postshock* conditions of the main bow. The filling factor is assumed to be small, consistent with the small lumps seen in the bow in the WFPC2 images (Heathcote et al. 1996).

Table 2 shows the results of adding a $25\,\mathrm{km\,s^{-1}}$ shock onto the main $80\,\mathrm{km\,s^{-1}}$ shock with a preshock density of $10^5\,\mathrm{cm^{-2}}$, a preshock magnetic field of 800μG, and an area filling factor of 40 percent. The same diagnostic line ratios were used to check the correct parameters as in the baseline model. This superposition model accurately reproduces the observed forbidden line ratios and lines fluxes above 4000 Å. The predicted ratios are not perfect due to the large uncertainties in the location of the secondary shocks in the postshock region of the main bow (affecting the secondary's preshock density and magnetic field), uncertainties in the viewing angle of the secondary shock, the extreme sensitivity of these emission line ratios to density at small shock velocities, and the rather arbitrary area filling factor. Clearly, this shock cannot be modeled by a single-velocity plane parallel shock. The success of the secondary shock model at reproducing the data indicates that there is in fact a mixture of high and low shock velocities in the beam.

There are at least two plausible explanations for the existence of a secondary shock in the HH 47A working surface. First, a small, unusually dense cloud in the preshock medium can pass through the main bow intact and have its density enhanced. If these clouds are sufficiently dense they can form a slow shock with the ordinary

TABLE 1

OBSERVED EMISSION LINES (Hβ = 100)[a]

	Bowshock			Mach Disk		
Identification	Observed Wavelength	Observed Flux	Dereddened Flux	Observed Wavelength	Observed Flux	Dereddened Flux
	...	...		2324.22	150 (2)	350 (5)
C II] 2325.07	2325.39	430 (4)	1000 (10)	2326.04	bl w/2323	
Si II]	2334.05	34 (1)	80 (3)	...	...	...
[Fe II]	2381.9	200 (2)	410 (5)	2381.92	75 (2)	160 (5)
[Fe II]	2625.73	200 (2)	390 (5)	2625.55	66 (1)	130 (3)
[Fe II]	2631.24	30 (1)	60 (3)	2629.86	8 (2)	15 (5)
Mg II 2795.74	2795.5	1200 (12)	1920 (20)	2795.44	370 (4)	600 (10)
Mg II 2802.91	2802.94	640 (6)	1020 (15)	2802.64	200 (3)	320 (8)
	2967.5	70 (12)	100 (20)	2967.83	15 (2)	22 (5)
[O II] 3729.44	3730.67	110 (2)	140 (3)	blend	90 (1)	110 (3)
H8 3889.28	3890.86	9 (2)	11 (4)	3891.59	5 (1)	6 (3)
Ca II 3933	3934.89	90 (2)	105 (5)	blend	25 (1)	30 (4)
Ca II 3968.73	3969.84	75 (2)	88 (5)	3967.82	29 (1)	35 (3)
+ Hϵ3970.30						
[S II] 4068.66	4069.59	100 (2)	120 (5)	4069.14	20 (2)	23 (5)
[S II] 4076.72	4077.34	17 (5)	20 (8)	4076.93	10 (1)	11 (3)
Hδ 4101.97	4104.02	17 (2)	20 (3)	4102.37	23 (2)	20 (5)
[Fe II]	4244.64	25 (2)	29 (3)	blend	...	...
[Fe II]	4287.84	38 (2)	44 (3)	4286.55	7 (1)	7 (3)
Hγ 4340.71	4342.37	42 (2)	47 (3)	4340.63	25 (2)	28 (5)
[Fe II]	4359.33	24 (2)	29 (3)	...	...	...
[Mg I] 4562.90	4563.44	13 (2)	14 (3)	4562.79	6 (1)	6 (3)
[Mg I 4571.39	4571.48	47 (2)	50 (3)	blend	13 (5)	14 (10)
[Fe II]	4776.18	7 (2)	7 (3)	...	...	...
[Fe II]	4813.96	12 (2)	12 (3)	...	...	...
Hβ 4861.58	4862.6	100	100	4861.85	100	100
[Fe II]	5112	9(1)	9 (2)	...	...	...
[Fe II]	5158.30	48(5)	46 (8)	...	...	...
[N I] 5200.97	5200.72	220 (4)	210 (6)	5198.15	60 (5)	57 (10)
[Fe II]	5262.29	29 (2)	26 (4)	5259.74	15 (3)	14 (6)
[Fe II]	5272.80	9 (2)	9 (4)	5273.55	6 (1)	5 (3)
[Fe II] 5527	5529.33	12 (4)	11 (6)	...	...	...
[O I] 6300.74	6300.54	570 (6)	470 (8)	6300.11	150 (3)	120 (5)
[O I] 6364.32	6363.58	210 (4)	170 (8)	6362.85	43 (1)	35 (3)
Hα 6562.75	6563.05	530 (5)	420 (10)	6562.12	430 (4)	340 (7)
[N II] 6584.28	6584.95	100 (1)	79 (3)	blend	49 (3)	39 (5)
[S II] 6717.44	6715.62	630 (6)	490 (15)	6715.10	150 (2)	120 (5)
[S II] 6731.69	6731.62	850 (9)	670 (18)	6729.43	190 (2)	150 (5)

[a]Dereddened with a standard galactic reddening curve, $E_{(B-V)}$=0.18

TABLE 2

MODELED EMISSION LINES (Hβ = 100)

Line/Ratio	Observed	Baseline Model Predicted	Secondary Model Predicted
[N II] 6584.28 / Hα	0.215	0.166	0.118
[N II] 6584.28 / [O I] 6300.74 + 6364.32	0.14	2.0	0.222
[N I] 5200.97 / [N II] 6584.28	2.33	0.064	2.91
[O I] 6300.74 + 6364.32 / Hα	1.53	0.083	3.12
[S II] 6717.4 + 6731.69 / hα	2.77	0.172	4.2
[S II] 6717.44 / [S II] 6731.69	0.743	0.753	0.604
C II] 2325.07	996	12.7	69
Si II]	79	2.2	19.9
Mg II 2795.74 + 2802.91	1921	41.8	838
[O II] 3729.44	136	67	63
Ca II 3933 + 3968.73	193	5.7	590
[S II] 4068.66 + 4076.72	123	4.54	164
Hβ 4861.58	100	100	100
[N I] 5200.97	210	1.65	86.7
[O I] 6300.74 + 6364.32	470	26	979
Hα 6562.75	417	313	313
[N II] 6584.28	79	52	58
[S II] 6717.44	494	23.2	500
[S II] 6731.69	665	30.8	821

postshock gas in the cooling region. Second, two of these denser clouds can collide in the post-bow region, producing a slow shock. The effect can occur only inside the main bow. Whatever the cause, it is clear that only a mixture of different shock velocities in the bow can explain the observed forbidden line ratios.

4. THE TWO-PHOTON CONTINUUM

The two-photon continuum is a well-known emission process in low-excitation shocks (Spitzer & Greenstein 1951). Since the preshock density and ionization fraction determine the population of electrons in the $^2S_{\frac{1}{2}}$ level, the total luminosity of the two-photon emission constrains the density and ionization state of the preshock gas.

The continuum emission in the two spectra was averaged over 50 Å bins chosen to avoid all known emission lines. These dereddened, binned continua appear in Figure 2 along with the expected two-photon continuum distribution,

$$\frac{F_\nu}{\nu} \sim \left[\left(\frac{\nu}{\nu_T}\right)\left(1-\frac{\nu}{\nu_T}\right)\right]^{0.5}, \quad (1)$$

where ν_T is the photon frequency corresponding to the 10.2 eV energy of the $^2S_{\frac{1}{2}}$ level (Brugel, Shull, & Seab 1982). The Mach disk continuum matches well with the expected two-photon distribution, but the bow shock

spectrum is strongly enhanced in the UV. This enhancement hints at an instrumental effect because there are no known radiative processes, other than the two-photon neutral hydrogen decay, that could produce this spectrum. There are two possible instrumental explanations. Scattered light can produce a roughly flat distribution in raw counts which is enhanced in the blue by the pipeline flux calibration. It is also possible that an error in the flux calibration overcompensated for the decrease in detector sensitivity in this region of the spectrum. This overcorrection would also artificially enhance the emission lines in this region relative to unaffected optical lines, an effect which we observe here (see the Mg II lines in Table 2).

5. CONCLUSIONS

The results of this work are summarized below. A more complete discussion will appear in a future paper.

- These spectra have the longest wavelength range of any high signal-to-noise spectra taken of HH 47. They are the richest optical spectra to date of this object, with 36 identified emission lines. The iron lines alone represent a wealth of new information that awaits a model.
- A single velocity plane-parallel shock model best fits the observed line ratios for $V_s = 80 \pm 5\,\mathrm{km\,s^{-1}}$, $\log n_0 = 2.72 \pm 0.35\,\mathrm{cm^{-2}}$, and $B_o = 165 \pm 100\,\mu\mathrm{G}$. These results are consistent with previous estimates (Morse et al. 1994).
- The optical forbidden line fluxes are enhanced well above their predicted fluxes for a single $80\,\mathrm{km\,s^{-1}}$ shock. The strong forbidden lines can be explained if a lower velocity shock exists inside the main bow shock. Such secondary shocks can arise from density variations in the preshock medium colliding with the cooled and condensed postshock gas, or they can arise from two such clouds striking each other.
- The optical/UV continuum seen by other observers is also seen here in the Mach disk and bow shock. The Mach disk spectrum matches that expected from two-photon emission, but the bow shock deviates from the expected distribution at the bluest wavelengths. We have not ruled out an instrumental effect to explain this deviation.

REFERENCES

Brugel, E. W., Shull, J. M., & Seab, C. G. 1982, ApJ, 262, L35
Hartigan, P. M., Morse, J. A., & Raymond, J. C. 1994, ApJ, 436, 125.
Heathcote, S., Morse, J. A., Hartigan, P. M., Reipurth, B., Schwartz, R., Bally, J., & Stone, J. M. 1996, AJ, 112, 1141
Morse, J. A., Hartigan, P. M., Heathcote, S., Raymond, J. C., & Cecil, G. 1994, ApJ, 425, 738
Raymond, J. 1979, ApJS, 39, 1
Spitzer, L., & Greenstein, J. L. 1951, ApJ, 115, 407